J. Indian Soc. Coastal Agric. Res. 41(1): 24-40 (2023) https://doi.org/10.54894/JISCAR.41.1.2023.129996

Assessing the Seasonal Crop Acreage in the Ganges Delta Using Multi-Temporal Sentinel-2 Data: A Case Study in Gosaba CD Block

M. K. NANDA[1], A. GHOSH[1,2]*, D. SARKAR[1], S. SARKAR[3], K. BRAHMACHARI[4], K. RAY[5], R. GOSWAMI[3] and M. MAINUDDIN[6]

[1]Department of Agricultural Meteorology and Physics, Bidhan Chandra Krishi Viswavidyalaya, Mohanpur - 741 252, West Bengal, India
[2]Department of Agricultural Meteorology, Odisha University of Agriculture and Technology, Bhubaneswar - 751 003, Odisha, India
[3]Integrated Rural Development and Management Faculty Centre, Ramakrishna Mission Vivekananda Educational and Research Institute, Narendrapur - 700 103, West Bengal, India
[4]Department of Agronomy, Bidhan Chandra KrishiViswavidyalaya, Mohanpur - 741 252, West Bengal, India
[5]Sasya Shyamala Krishi Vigyan Kendra, Ramakrishna Mission Vivekananda Educational and Research Institute, Arapanch, Sonarpur - 700 150, West Bengal, India
[6]CSIRO Land and Water, Canberra, ACT - 2601, Australia

Received: 09.11.2022 Accepted: 31.05.2023

The present study assessed the seasonal and inter-annual variation in cropping pattern and crop acreage during summer (mid-February to May) and winter (November to January) seasons of 2017-2018, 2018-2019, and 2019-2020 cropping years over the Gosaba Block of Indian Sundarbans. Multi-temporal Sentinel-2 images acquired during the critical crop growth stages during a particular season were taken together for classification instead of a single image classification approach. This study employed the random forest algorithm for image classification for seasonal crop-fallow mapping over three consecutive years. The estimated post-monsoon (winter) crop coverage was less than that in the pre-monsoon (summer) season. In the post-monsoon season crop coverage varied from 3% to 12% of the net cultivable area, whereas pre-monsoon season crop coverage varied from 23% to 42%. The estimated area under *boro* rice decreased in 2018-19 and 2019-20 with a simultaneous increase in non-rice crops. Seasonal fallow land showed wide inter-annual variation. The amount and distribution of rainfall during the last part of the monsoon season and in the following months had a strong influence on the cropping pattern of the Sundarbans region. Results clearly showed that winter crop coverage gradually decreased over the study period depending on the rainfall pattern in the monsoon season and in the following months. During summer season, the area under non-rice crops notably increased at the cost of the area under *boro* rice. These findings clearly indicated the farmers' preferences for cultivating crops according to the climatic variability. The present study may be helpful for cropping intensification in the threatened regions for achieving sustainability.

(***Key words:*** *Crop coverage, Indian Sundarbans, Post and pre-monsoon, Sentinel-2, Random forests classification*)

Eliminating hunger from the world is one of the prime concerns in recent times. Out of the seventeen Sustainable Development Goals (SDGs) of the United Nations (UN), the second goal aims at achieving zero hunger and ensuring food security through sustainable practices, by 2030 (Blesh *et al.*, 2019). To meet the food demand of the ever-increasing world population, agriculture in the stressed regions should come under focus. Indian Sundarbans, part of the world's largest continuous tidal halophytic mangrove forest, is one of the most threatened regions of the world from ecological and climatological view points (Samanta and Hazra, 2012; Debnath, 2018). Agriculture is the primary source of income, engaging over 65% of the population staying in this region. However, crop production has been constrained by poor drainage facilities causing an extended period of water logging during the monsoon season followed by the rapid build-up of soil salinity and scarcity of fresh water for irrigation during the dry season. The frequent occurrence of tropical cyclones has made agriculture a risky enterprise (Bell *et al.*, 2019; Mainuddin *et al.*, 2019a, 2019b; Ghosh *et al.*, 2019; Ray *et al.*, 2019; Sarkar *et al.*, 2019; Sarkar *et al.*, 2020).

**Corresponding author:* E-mail: ghoshargha4@gmail.com

Remote sensing has been demonstrated as an effective tool for monitoring cropping practices. Satellite remote sensing has entered a new era with the launching of the high-resolution optical sensor Sentinel-2 by the European Space Agency as a part of their Copernicus program. The multispectral instrument (MSI) of the Sentinel-2 generates multi-band images at 10 m, 20 m, and 60 m spatial resolutions in a 5 days repeat cycle with a swath of 290 km (Ramoelo *et al.*, 2015; Veloso *et al.*, 2017). Sentinel-2 data collected during different seasons can be successfully employed to represent the cropping scenario in a given region (Ghosh *et al.*, 2019).

The present study aimed to assess the seasonal crop acreage of Gosaba Block in the Indian Sundarbans. We used multi-temporal Sentinel-2 images corresponding to pre-monsoon (summer) and post-monsoon (winter) seasons of three consecutive cropping years *viz.*, 2017-18, 2018-19, and 2019-20. The crop development pattern was determined by studying the temporal profile of Normalised Difference Vegetation Index (NDVI). Random Forest Classification (RFC), the supervised machine learning algorithm was employed to estimate the spatio-temporal dynamics of cropped and fallow land during the study period.

MATERIALS AND METHODS

Study area

The Gosaba Block of Indian Sundarbans spreads over a 29,500 ha area extending from 22° 3′ N to 22° 15′ N and from 88° 42′ E to 88° 60′ E in South 24 Parganas district of West Bengal, India (Fig.1).

The district's climate is humid subtropical, with an annual rainfall of about 1800 to 2000 mm. The last 30 years of rainfall data show that a significant part (74%) of rain occurs during the monsoon season extending from June to September (IMD, 2020). Fig. 2 presents the monthly rainfall during the study period (May 2017 to April 2020). For this study, we have used the rainfall data recorded from the Decagon High-Resolution Rain Gauge (ECRN-100), fixed on the Automatic Weather Station installed in the study site under the CSI4CZ Project of the Australian Centre for International Agricultural Research (ACIAR). The satellite-derived CHIRPS daily rainfall data product (https://developers.google.com/earth-engine/datasets/catalog/UCSB-CHG_CHIRPS_DAILY) was used for gap-filling against the missing data.

Satellite data and source

Multi-temporal Sentinel-2 data (https://scihub.copernicus.eu/dhus/#/home) were collected from the open data archive of the European Space Agency via Copernicus Sci-hub. Sentinel-2, being an optical sensor provides cloud-free data only during the non-rainy seasons. The acquisition dates of Sentinel-2 data used in the study are depicted in Table 1. Cloud interference and atmospheric haze caused quality issues with some of the satellite data. The clear sky images were therefore used for subsequent analysis.

Field survey

A periodic field survey through transect-walk across the crop fields was conducted in the Gosaba Block using a hand-held GPS device to select training sites and test the classification accuracy. The dates of the field survey are given in Table 1. During the field survey, detailed phenological and operational calendars of each crop in the cropping systems were collected from the local farmers. The stratified random sampling method was followed to get representative samples (Fig.1) from different cropping systems. The samples were selected considering the spatial distribution of crops and cropping systems in the study area as informed by the local community as far as possible. At least sixteen pixels from every cropping system and the other land-use features were taken as the training class for extracting the spectral reflectance and classification. The field survey revealed that during monsoon seasons mostly paddy was cultivated in the crop fields. The farmers grew wide varieties of winter vegetables, including potato, cauliflower, cabbage, knol-khol, and tomato during the post-monsoon season. During the pre-monsoon (summer) season, vegetables like okra, chilli, and Indian spinach were grown.

Pre-processing of satellite images

The Sentinel-2 images (Level-1) were pre-processed for atmospheric correction (haze removal) and radiometric correction to get ground reflectance at different wavebands. We used only visible and near-infrared (VNIR) bands for classification and stacked together the VNIR spectral bands for each image. Then we applied geometric correction using GPS-recorded ground control points spread over the study region.

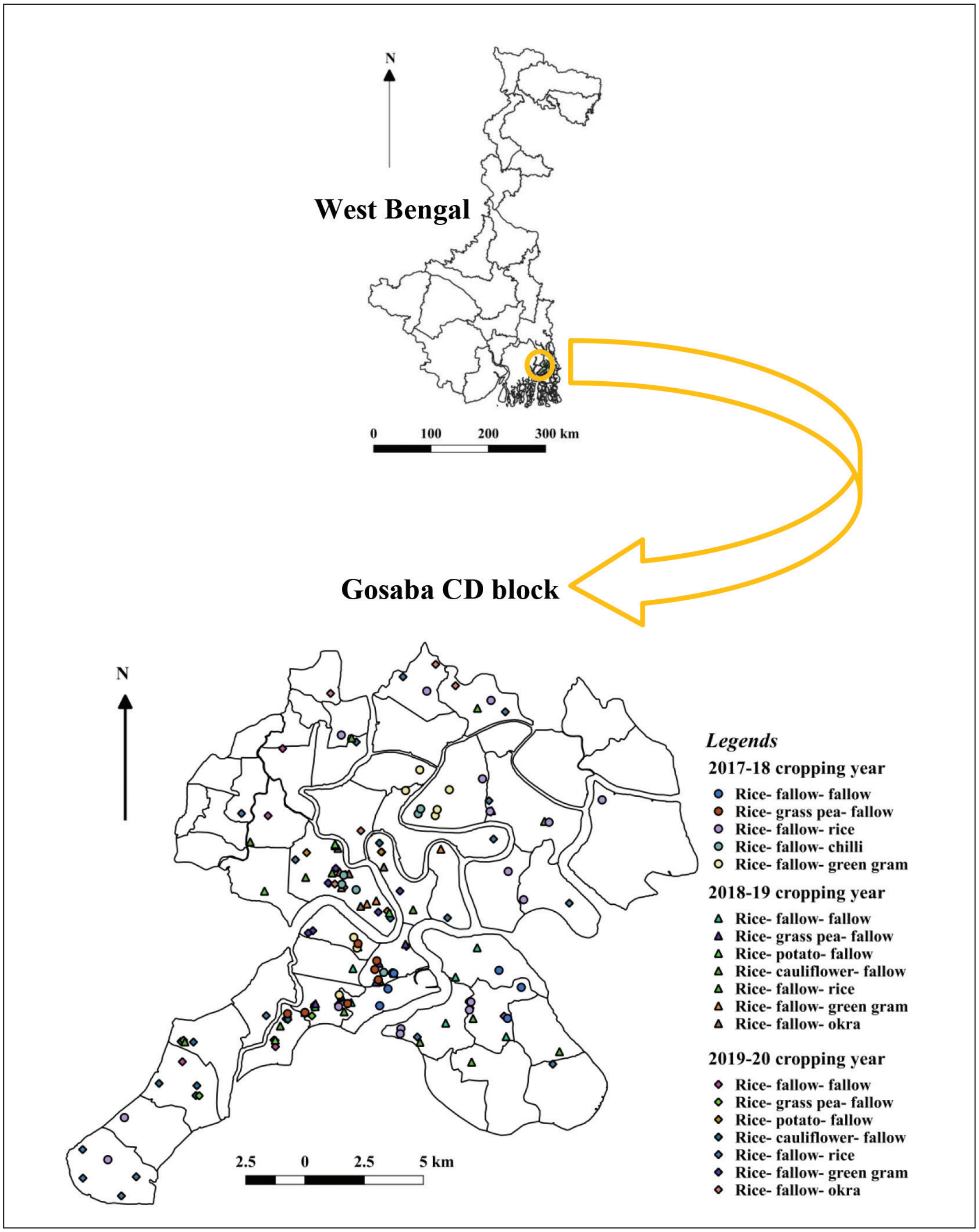

Fig. 1. *Study location (Gosaba CD Block of West Bengal, India) and survey sites*

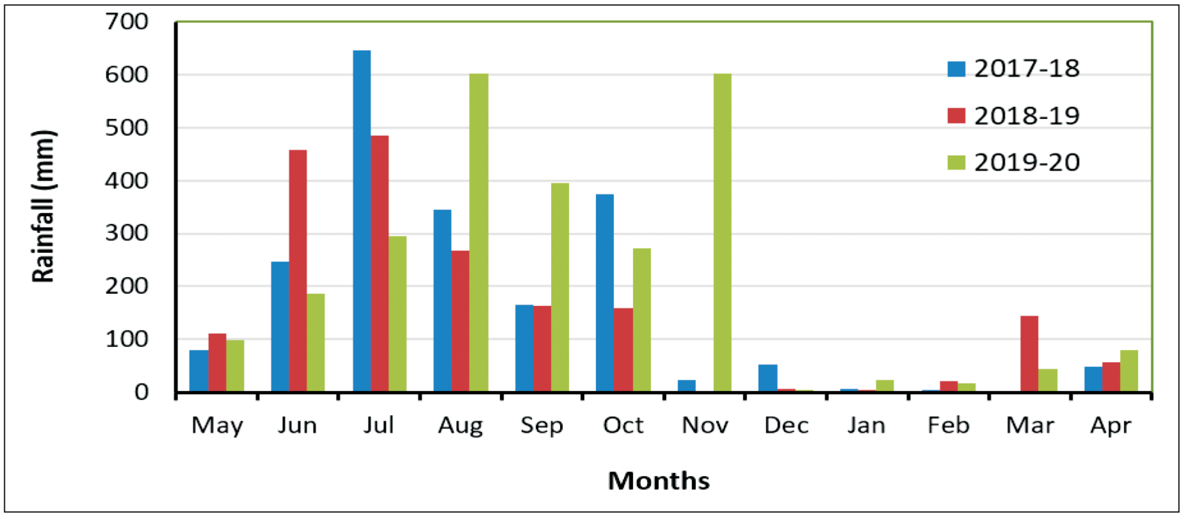

Fig. 2. *Monthly rainfall of Gosaba block during the study period*

Table 1. *Dates of satellite imageries acquisition and field survey for cropping system study*

Cropping year	Dates of satellite imageries acquisition		Dates of field survey
	Used for classification	Used for spectral profile study	
2017-18	Post-monsoon (winter): 16 Dec, 2017 30 Jan, 2018 4 and 14 Feb, 2018 Pre-monsoon (summer): 14 Feb, 2018 1 and 21 Mar, 2018 15 Apr, 2018	11 Nov, 2017 1 and 26 Dec, 2017 5, 10, 15 and 30 Jan, 2018 4 and 14 Feb, 2018 1, 11 and 21 Mar, 2018 15 Apr, 2018	15 Nov, 2017 12 Dec, 2017 25 Jan, 2018 21 Feb, 2018 30 Mar, 2018
2018-19	Post-monsoon (winter): 26 Dec, 2018 30 Jan, 2019 4 and 14 Feb, 2019 Pre-monsoon (summer): 14 Feb, 2019 21 and 26 Mar, 2019 15 Apr, 2019	7, 17, 22 and 27 Oct, 2018, 11 and 16 Nov, 2018 1, 11, 21 and 26 Dec, 2018 5, 20, 25 and 30 Jan, 2019 14 and 24 Feb, 2019 1, 21 and 26 Mar, 2019 15, 20, 25 and 30 Apr, 2019	10 Nov, 2018 21 Jan, 2019 20 Mar, 2019 10 Apr, 2019
2019-20	Post-monsoon (winter): 21 Dec, 2019 25 Jan, 2020 4, and 14 Feb, 2020 Pre-monsoon (summer): 29 Feb, 2020 10 and 30 Mar, 2020	27 Oct, 2019 11, 16 and 21 Nov, 2019 6, 11, 21 and 31 Dec, 2019 10 and 15 Jan, 2020 4, 14 and 19 Feb, 2020 10, 15, 20, 25 and 30 Mar, 2020 9, 14 and 19 Apr, 2020	27 Oct, 2019 6 Dec, 2019 25 Feb, 2020 6 and 14 Mar, 2020

Image sub-set, representing the study area was extracted from the stacked images by using the shapefile of the Gosaba block. The image pre-processing steps have been demonstrated in Fig. 3 in open-source QGIS-3.4.5 software.

Generation of spectral profile of cropping systems

The spectral reflectance pattern for different cropping systems was extracted using the zonal mean of training sites corresponding to the cropping systems as delineated through periodic field surveys. The images used for the preparation of the spectral profile are given in Table 1. We used the following formula to compute the temporal NDVI of crops and cropping systems (Rouse *et al.*, 1974) –

$$NDVI = \frac{R_{NIR} - R_R}{R_{NIR} + R_R}$$

The NDVI represents the canopy growth of the crop, where R_{NIR} = Reflectance in the near-infrared (NIR) band and R_R = reflectance in the red band. The value of NDVI ranges from -1 to +1.

Random forests classification

The present study employed the machine learning random forests classification (RFC) technique to classify Sentinel 2 images. The RFC is an ensemble decision tree classifier developed by Breiman (2001), which works

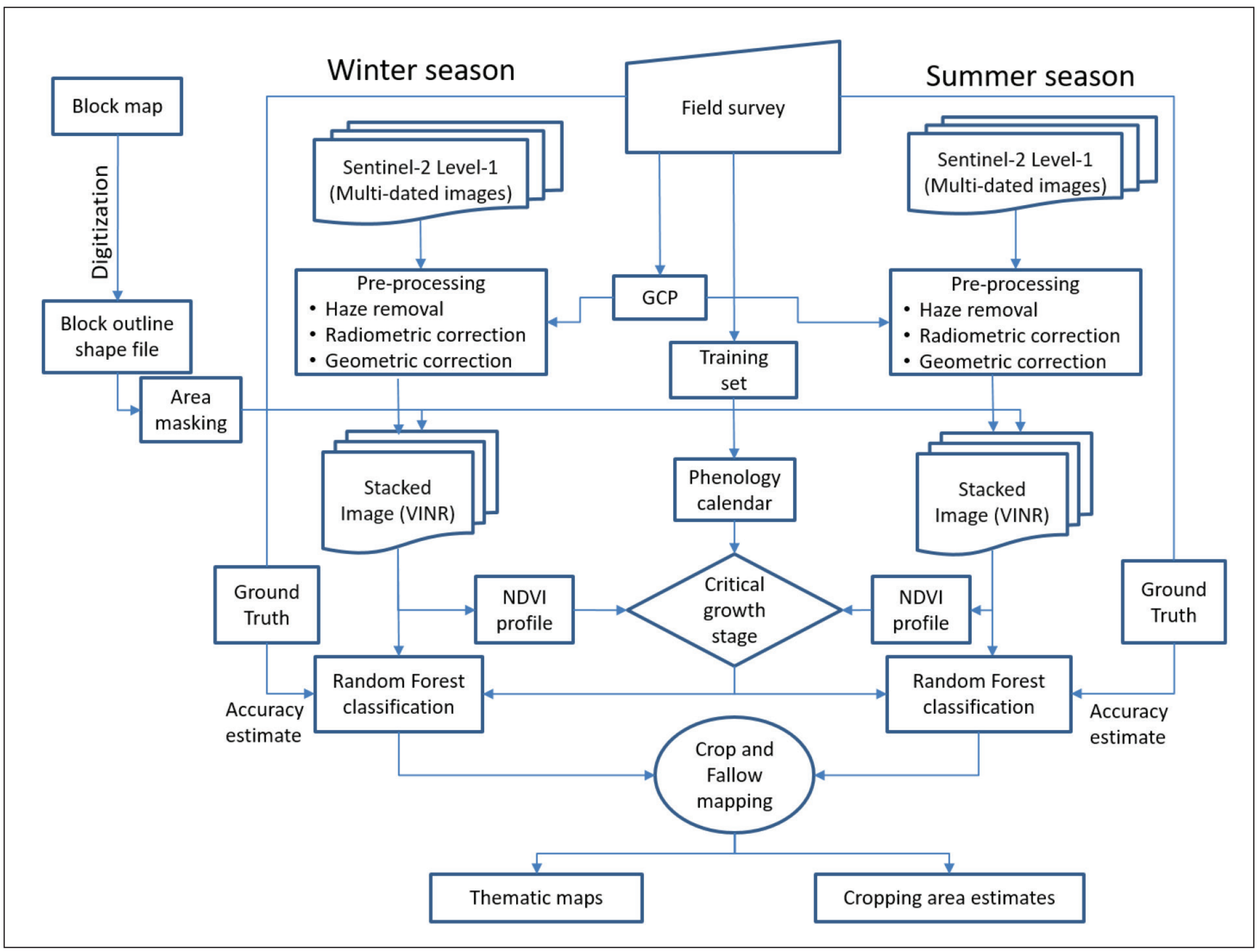

Fig. 3. *Model framework demonstrating image processing and analysis for seasonal land use mapping*

by 'growing' many individual decision trees. Breiman defined random forests as a classifier consisting of a collection of tree-structured classifiers {h(x,Θk), k = 1, 2, . . . }, where the {Θk} are independent identically distributed random vectors, and each tree casts a unit vote for the most popular class at input x. The total number of votes determines the final classification response (class assignment) from all of the trees *i.e.,* the class predicted most is the class that is assigned for that object.

The advantages of RFC lie in its ability to handle a large number of training sample units and measure each input variable into importance levels. The RFC increases the diversity of the trees by making them grow from different training data subsets created through bootstrap aggregating or "bagging". It is free from the assumption of normal distribution and robust to outliers and noise (Rodriguez-Galiano *et al.*, 2012). These advantages provide a strong argument for choosing the RFC technique for classifying multi-temporal satellite images. Sentinel-2 images, corresponding to the critical crop growth stages were determined from the spectral reflectance profile and selected as input (bands stack containing VNIR bands) for RFC. Sentinel-2 images acquired at the critical crop growth stages were selected for each season and taken together for land use classification of the corresponding season. The same procedure was followed for the two seasons in every cropping year. So the results obtained from the multi-image classifications were not the land use pattern on a single date but during that particular cropping season.

The random forest classification was done in open-source SAGA (System for Automated Geoscientific Analysis, SAGA 6.4.0) software. The different land use classes included croplands, fallow lands, water bodies, treesand settlements, mangroves, and wetland/puddled fields during the winter season. The summer croplands were subdivided into rice and non-rice crops. The non-rice crops included green gram and summer vegetables like okra and Indian spinach. The settlement areas in the study site are generally associated with homestead plantations where the small houses are often partially covered by tree canopies. Hence, a combined class of "trees + settlements" was used in the present classification scheme. A similar approach was followed earlier by Samanta and Hazra (2012) and Haldar and Debnath (2014). The mangrove, on the other hand, with its dense and contiguous canopy structure, was well distinguished from the homestead plantation.

Accuracy assessment

To assess the classification accuracy confusion matrix was generated for each classification. We calculated the producer's, user's, and overall accuracy of the classification maps against the ground truth data (collected by stratified random sampling). Kappa test for the stratified random sampling was performed to examine the extent of agreement between predefined producer ratings and user-assigned ratings (Stehman, 1996).

RESULTS AND DISCUSSION

Spectral response of cropping systems

The temporal NDVI profiles of different cropping systems were generated for the period extending from end-October to mid-April of the three cropping years, 2017-18, 2018-19, and 2019-20 and the results so obtained have been presented in Fig. 4. A clear distinction between crop and fallow period in the NDVI profile was observed. The NDVI of rice at the peak growing phase exceeded 0.6, whereas, during the fallow period, the NDVI was less than 0.2. On the other hand, the non-rice crops attained NDVI value in the range of 0.4 to 0.5 at the peak vegetative phase depending upon the canopy density and growth phase. Although there was no distinct difference in the NDVI pattern among non-rice crops, one could distinguish them by their respective growing window.

The rice-fallow-fallow system (mono-cropping of rice) recorded the peak NDVI during mid-October and decreased after that to reach the minimum value in the first week of December in all the three cropping years. During the fallow period, the NDVI ranged from 0.14 to 0.21 depending on the condition of stubbles left in the field. Sometimes stubble growth after rice harvest, specifically after a spell of rain, led to an increase in NDVI, which might appear similar to short-duration crop canopy in the satellite imageries. On the other hand, the NDVI profile of the rice-fallow-rice system showed a bimodal pattern with a second peak from the end of March to mid-April. The rice crop showed a low NDVI (less than 0.01) during the transplanting phase in the puddled field in January-February, which then increased to reach a peak value (more than 0.6) during the active vegetative phase at the end of March to April. Then, the NDVI decreased abruptly as the crop reached maturity and the plant dried up (Fig. 4). The NDVI pattern of the rice-grass pea-fallow system depended upon the system of grass pea cultivation. In 2017-18, the grass pea was successfully grown as *utera* crop, and the NDVI remained at 0.4 or above till the first week of February. In the following years, the *utera* crop failed, and grass pea was broadcasted again after the rice harvest. As a result, the NDVI reached the lowest value during mid-December and increased after that as a result of the grass pea's growth reaching a second peak during the first week of February. The rice-fallow-chilli, rice-fallow-okra, and rice-fallow-green gram, systems also showed bi-modal patterns of NDVI similar to that of the rice-fallow-rice system. However, the peak NDVI value of the non-rice crop was in the range of 0.40 to 0.45, much lower than that of rice (0.60). In some fields, summer vegetables, including mixed cropping of Indian spinach and okra were grown after harvesting potato and

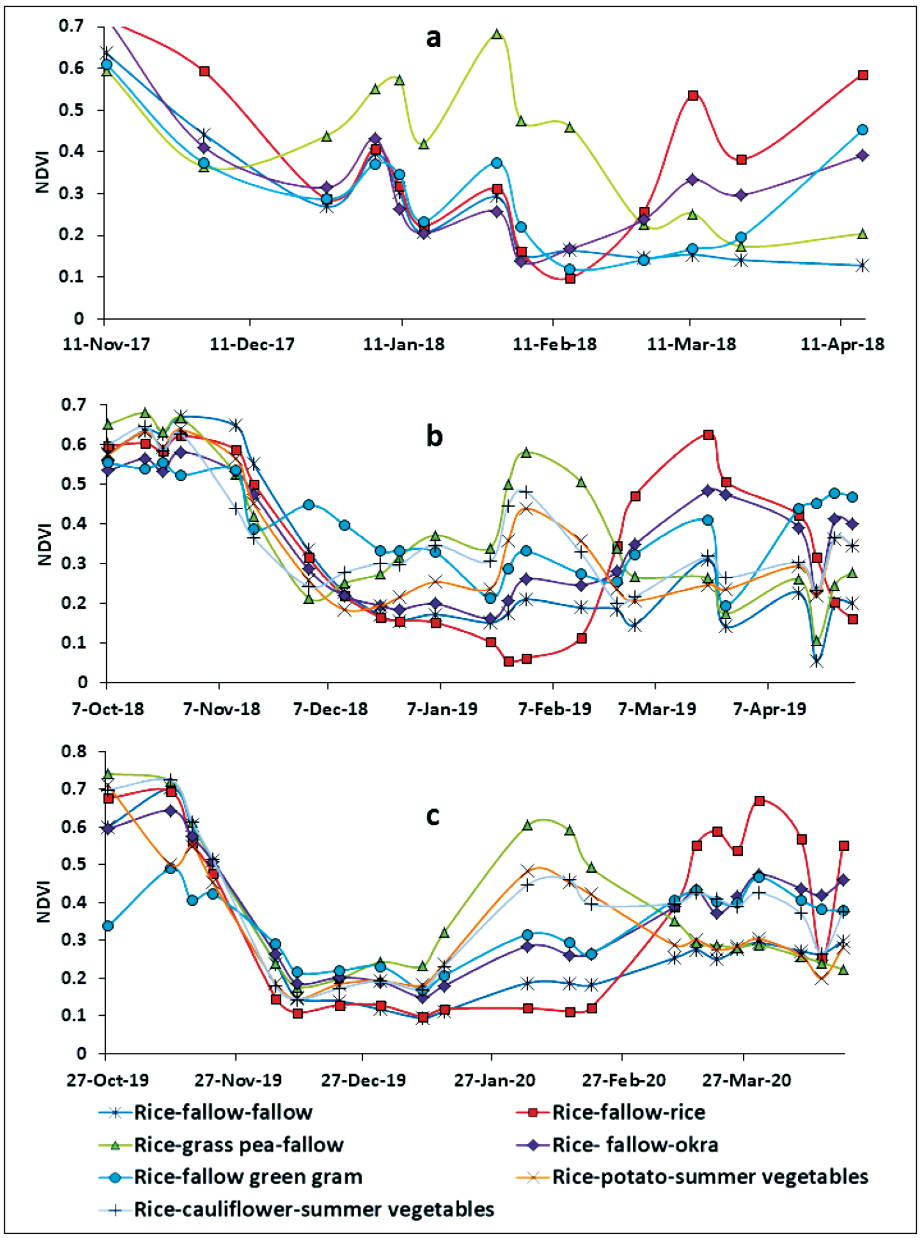

Fig. 4. *Temporal NDVI profile of different cropping systems during (a) 2017-2018 (b) 2018-2019 and (c) 2019-2020 cropping years*

cauliflower. Therefore a slight increase in NDVI profile was observed during the summer season. However, the scale of this practice was very limited.

The spectral reflectance of vegetation represents its growth and vigour. It was observed that a healthy canopy exhibited higher reflectance in the NIR band.The high absorption of the NIR band by water (Sahu, 2014; Mondejar and Tongco, 2019) and more reflection of the visible band by dry soil help in assessing canopy density in dry or moist soil background. The study showed that the cropping window and growth pattern of individual crop components of a cropping system are most precisely represented by the temporal profile of NDVI. The Sentinel-2 constellation of satellites that provides images of high spatial resolution at frequent intervals offers the capability to capture the periodic growth and phenological development of individual crops and hence is suitable for the cropping system analysis (Ghosh *et al.*, 2022). The NDVI during the puddling and transplanting stage of *boro* rice appeared to be very low compared to dry soil, which formed the basis of distinguishing rice from other arable crops. The crop monitoring potential of Sentinel-2 imageries in a similar context was reported earlier. The Sentinel-2 data has been found effective in assessing crop growth patterns associated with different cropping systems because of its fine spatial resolution and frequent revisiting period (Veloso *et al.*, 2017; Mandal *et al.*, 2018).

Inter-annual variability of cropped and fallow land

Since the study used multi-temporal images in RFC, the classified output did not represent the land useland cover situation of a particular date but for the

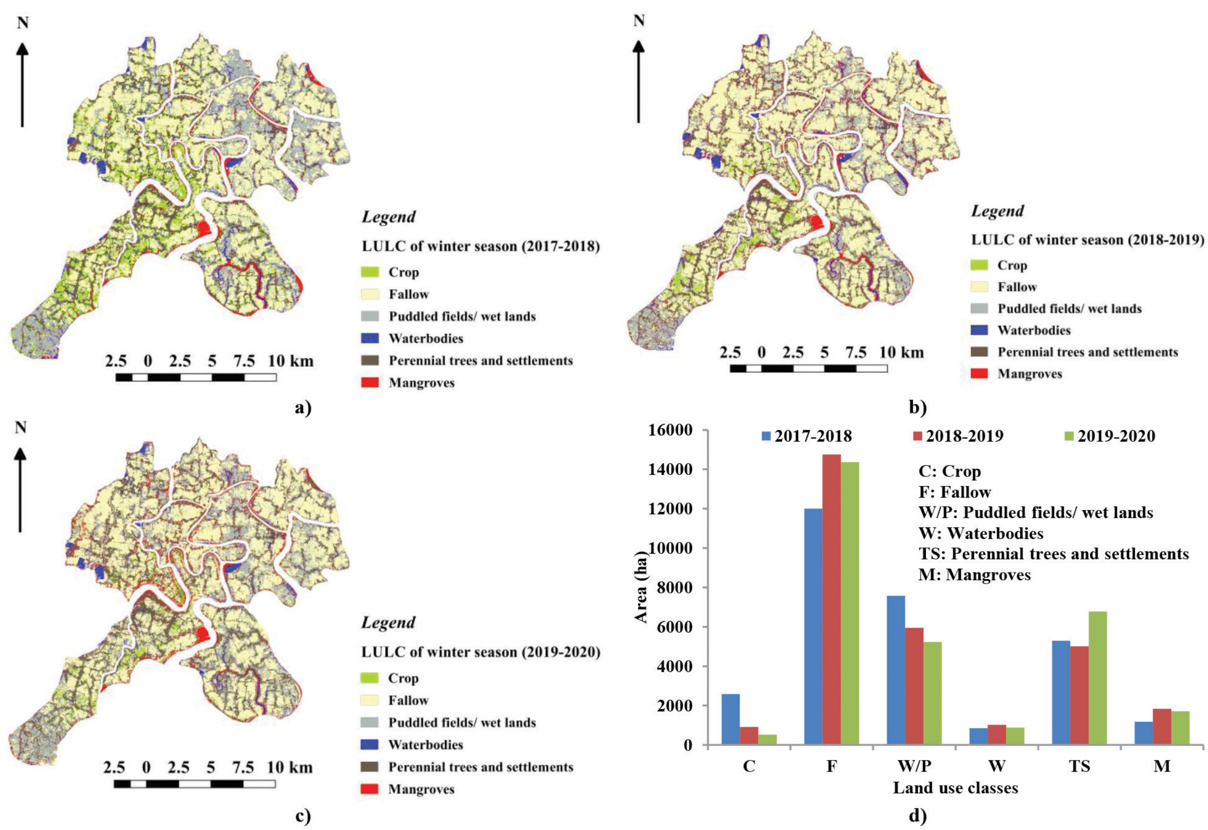

Fig. 5. *Land use map of Gosaba block during the post-monsoon (winter) season of (a) 2017-2018; (b) 2018-2019 and (c) 2019-2020 cropping year (d) Changes in the land use areas in the winter seasons during the three cropping years*

entire season. The land-use classification maps for the winter season of 2017-18, 2018-19, and 2019-20 have been represented in Fig. 5. We estimated the cultivable lands consisting of croplands, seasonal fallow, and wetlands/puddled fields to be about 75%, 73%, and 68% of the total area of Gosaba Block in 2017-18, 2018-19, and 2019-20, respectively, against 25%, 27% and 32% under non-agricultural land use classes including mangroves, water bodies, and trees + settlements. A significant part of the non-agricultural lands comprised of trees + settlements class. The area under the mangrove and water body was much less than trees + settlements with slight inter-annual variations. On the other hand, there was a noticeable increase in the area under trees + settlements in 2019-20.

In the summer season, the agricultural land i.e., the areas under boro rice and other arable crops (mainly green gram and summer vegetables) and fallow land occupied about 62.5%, 75.7%, and 60.7% of the total land during 2017-18, 2018-19, and 2019-20 whereas the non-agricultural land comprising of water bodies, trees + settlements and mangrove classes occupied 37.5, 24.3 and 39.3%, respectively in the corresponding years (Fig. 6).

The general trend showed that the fallow land occupied a major part of the cultivable area during the winter season. It was estimated that about 54.1% of total cultivable land remained fallow during the winter season of 2017-18. The fallow land percentage progressively increased to 68.3 and 71.4% during the winter season in the subsequent years (Fig. 5). On the other hand, the estimated area under winter crop decreased drastically from 2585 ha in 2017-18 to 902 ha in 2018-19 and to 525 ha in 2019-20. There was also a noticeable decrease in wetland and puddled fields during the same period.

The land-use statistics (Fig. 6) of the present study showed that the crop coverage area was much larger (23 to 42% of net cultivable land) in the summer season as compared to that of the winter season (2 to 12%). The

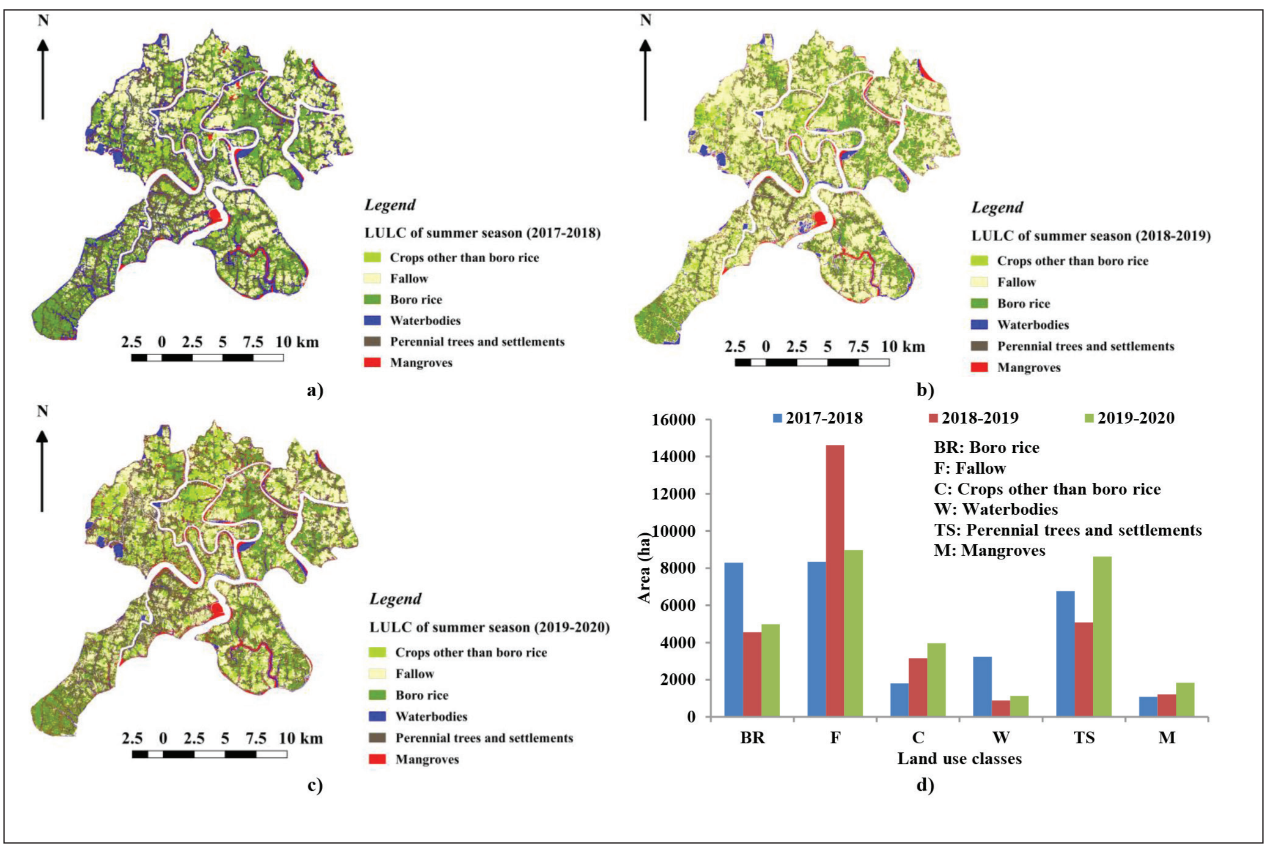

Fig. 6. *Land use map of Gosaba block during the pre-monsoon (summer) season of a) 2017- 2018; b) 2018-2019 and c) 2019-2020 cropping year d) Changes in the land use areas in the summer seasons during the three cropping years*

average estimated area under *boro* rice over the three years of study (2017-18 to 2019-20) was 5938 ha. The official estimate of the Government of West Bengal (2014) showed that the boro rice area of Gosaba block was 6440 ha. In the present study, we found a wide inter-annual variation of the area under *boro* rice cultivation. The estimated *boro* rice acreage in 2017-18 was 8289 ha which drastically reduced in the following years with 4545 ha in 2018-19 and 4979 ha in 2019-20. The inter-annual dynamics of summer rice and other arable crops like green gram and vegetables showed that while the summer rice areas reduced almost by 50% from 2017-18 to subsequent years, the cultivation of other non-rice crops increased progressively during this period. About 65.5% of cultivable land remained fallow in the summer season of 2018-19, which was much higher than in other years.

The present study revealed that a large proportion of land remained fallow during the winter and summer seasons which showed a very close agreement with the findings of Debnath (2018). Crop acreage was very low in the winter season as compared to that of the summer season. Furthermore, rice occupied a higher proportion of the area during the summer season than other summer crops. This was in agreement with the official estimate of the Government of West Bengal (2014). In the Indian Sundarbans region, the settlement areas are covered with perennial trees and that is why the settlement areas were considered together with the perennial vegetation in Indian Sundarbans areas during land use classification (Samanta and Hazra, 2012). The spectral signature of the trees matches that of the crops during active growing stages. This causes class mixing during land use classification (Ghosh *et al.*, 2019). Thus variation in the estimated area under tree and settlement area was found in the present study.

Accuracy of estimation

The classification accuracy of land use land cover (LULC) classes studied by comparing the classification results against the ground truth study revealed that the producer's accuracy of puddled fields/wetlands, water body, and mangroves was consistently significant (95% and above). In contrast, the user's accuracy was high in the waterbodies and mangroves classes during the winter season. Both producer's accuracy and the user's accuracy were comparatively lesser in fallow land during the winter season. The overall classification accuracy varied from 82% to 92%, whereas the Kappa value varied from 0.74 to 0.89 during the winter season (Table 2). In the LULC classification of the summer season, both producer's and user's accuracy was high in the case of mangroves (88% to 100%) and waterbodies (93% to 100%), and summer rice (95% to 100%) during the three years of study. The producer's accuracy of summer crops other than rice was very low (36%) during 2017-18. The overall classification accuracy during the summer season varied from 79% to 94%, whereas the Kappa value varied from 0.71 to 0.91.

Seasonal and inter-annual transformation between cropped and fallow land

The seasonal and inter-annual transformation between agricultural and non-agricultural land was estimated and presented by the thematic maps (Figs. 7 and 8). In between the first two successive winter seasons (2017-2018 to 2018-2019), about 3% (32.46 ha) and 13% (107.67 ha) area under water transformed to fallow land and wetlands/puddled fields, respectively (Table 3). A considerable change from cropland to fallow took place during this period. About 40% (1021.36 ha) of the cropland changed into fallow land and about 13% (1525.61 ha) of the fallow land changed into wetlands / puddled fields. About 1.5% (173.05 ha) of the fallow land was converted to cropped land. It was observed that about 15% (147.78 ha) and 19% (196.85 ha) of the water area in the winter of 2018-2019 changed into fallow land and wetlands/puddled fields, respectively in the winter of 2019-2020. About 31% (1835.45 ha) of the *boro* rice grown area was converted to fallow land. It was also observed that about 14% of the fallow land in 2018-2019 changed to cropland in the 2019-2020 summer seasons.

The summer season land use transformation showed that 260.72 ha of water class was converted to cropped land and 1770.2 ha of water class got converted to fallow land from 2017-2018 to 2018-2019 (Table 3). It was also found that about 13% and 38% of the *boro* rice area in the 2017-2018 cropping year transformed into other crops and fallow, respectively in the next summer season.

About 15% of summer fallow land was converted to cropland from 2017-2018 to the 2018-2019 cropping year. It was observed that about 4% of the water area

Table 2. *Classification accuracies of land use land cover classes in different cropping years*

Land use land cover of post-monsoon (Winter) season														
Year	Crop		Fallow		Wetlands/ puddled field		Waterbodies		Tree + settlements		Mangroves		OA	Kappa (KS)
	PA	UA	PA	UA	PA	UA	PA	UA	PA	UA	PA	UA		
2017-18	93.1	96.43	94.45	91.07	89.19	100	100	95.54	88.75	88.75	100	99.3	91.11	0.88
2018-19	66.96	100	89.23	89.23	99.89	96.22	100	96.43	98.94	100	99.43	100	81.61	0.74
2019-20	99.29	100	100	100	100	100	100	100	76.59	98.13	99.79	95.23	91.59	0.89
Land use land cover of pre-monsoon (Summer) season														
Year	Crop		Fallow		Wetlands/ puddled field		Waterbodies		Tree + settlements		Mangroves		OA	Kappa (KS)
	PA	UA	PA	UA	PA	UA	PA	UA	PA	UA	PA	UA		
2017-18	95.19	100	80.05	90.93	97.62	35.96	100	100	100	100	98.23	100	79.44	0.72
2018-19	99.71	99.8	100	100	100	100	100	92.86	86.67	97.85	100	100	80.07	0.71
2019-20	97.14	100	100	87.63	100	100	92.82	99.08	45.14	94.2	99.92	87.76	93.47	0.91

PA: Producer's accuracy (%); UA: User's accuracy (%); OA: Overall accuracy (%)

Table 3. *Change matrix of crop, waterbodies and fallow land during different cropping years*

Winter season					
	2018-2019				
2017-2018	Land use classes	Crop	Fallow	Wetlands/ puddled fields	Waterbodies
	Crop	450.62	1021.36	425.3	9.44
	Fallow	173.05	9855.9	1525.61	79.64
	Wetlands/puddled fields	90.87	3206.73	3102.45	265.08
	Waterbodies	0.08	32.46	107.67	531.5
	2019-2020				
2018-2019	Land use classes	Crop	Fallow	Wetlands/ puddled fields	Waterbodies
	Crop	209.25	266.29	33.94	0.22
	Fallow	126.33	11342.19	1933.25	79.66
	Wetlands/puddled fields	52.96	1835.45	2674.61	141.3
	Waterbodies	1.42	147.78	196.85	491.3
Summer season					
	2018-2019				
2017-2018	Land use classes	*Boro* rice	Crops other than *boro* rice	Fallow	Waterbodies
	Boro rice	3019.91	1101.03	3124.93	31.16
	Crop other than *boro* rice	219.03	466.19	990.55	8.42
	Fallow	466.84	755.28	6543.75	49.36
	Waterbodies	84.53	176.19	1770.15	571.71
	2019-2020				
2018-2019	Land use classes	*Boro* rice	Crops other than *boro* rice	Fallow	Waterbodies
	Boro rice	2923.65	276.65	403.71	30.3
	Crop other than *boro* rice	416.03	1061.4	806.67	7.95
	Fallow	971.89	2287.86	7106.55	528.82
	Waterbodies	31.85	5.05	224.21	495.4

in the summer of 2018-19 changed to cropland in the subsequent summer season. A conversion of 224.21 ha area from water to fallow was observed in this period. About 23% of the fallow land conversion to cropland was noticed between the summer seasons of 2018-2019 and 2019-2020 cropping years. Around 6% and 9% of the *boro* rice area in the 2018-2019 summer seasons changed to the other summer crops and fallow, respectively in the next season.

The seasonal dynamics of soil salinity and moisture status are the driving factors influencing the cropping system of the Sundarbans region. In the post-monsoon season, soil salinity was associated with the residual moisture content (Mainuddin *et al.*, 2019a,b). Hence, the amount and distribution of rainfall towards the end of the monsoon (September to October months) and rainfall due to cyclonic depression in the Bay of Bengal significantly influence the post-monsoon crop sequence in the coastal blocks of Sundarbans. Long-duration paddy is cultivated in this region, particularly in the low-lying areas where water remains stagnant until mid-November. This leaves limited scope for the cultivation of winter crops. The present study demonstrated the influence of rainfall distribution on cropping intensity. Compared to the following years, the higher winter crop

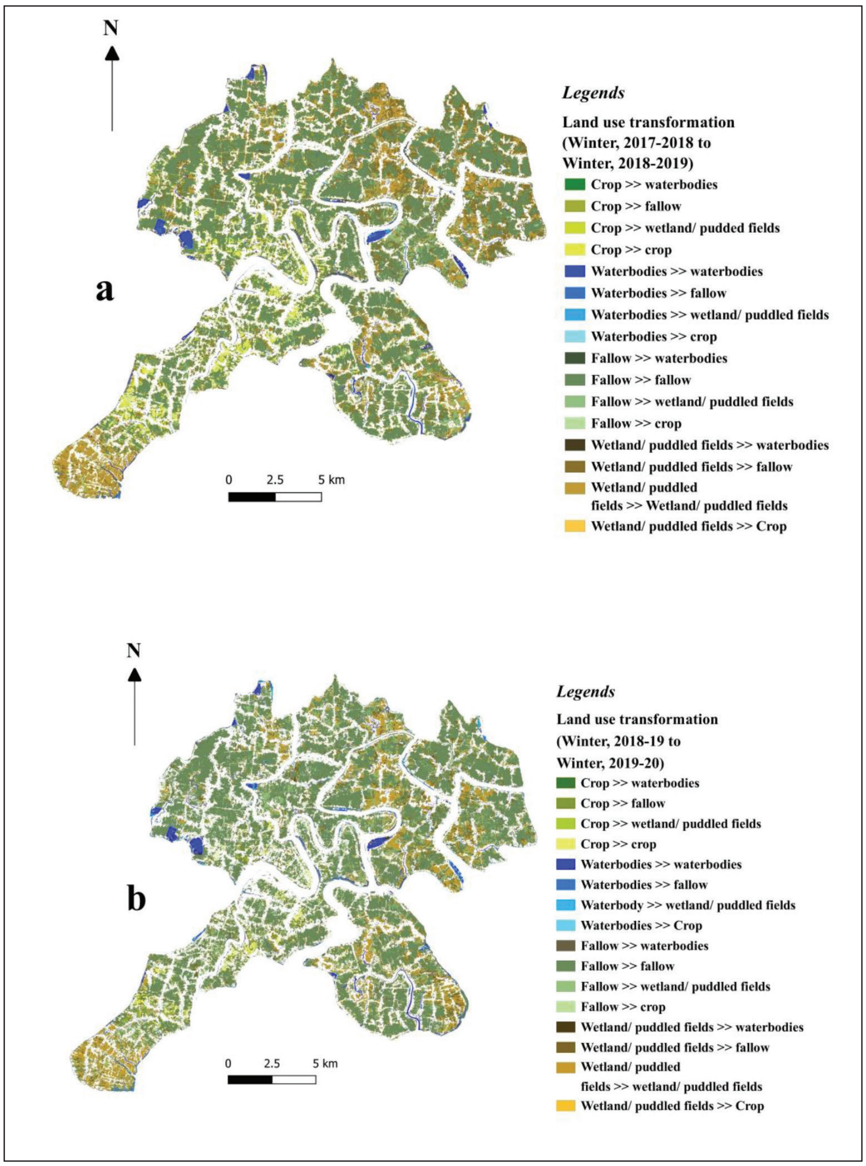

Fig. 7. *Post-monsoon (winter) season land use transformation a) 2017-2018 to 2018-2019 and b) 2018-2019 to 2019-2020 cropping years*

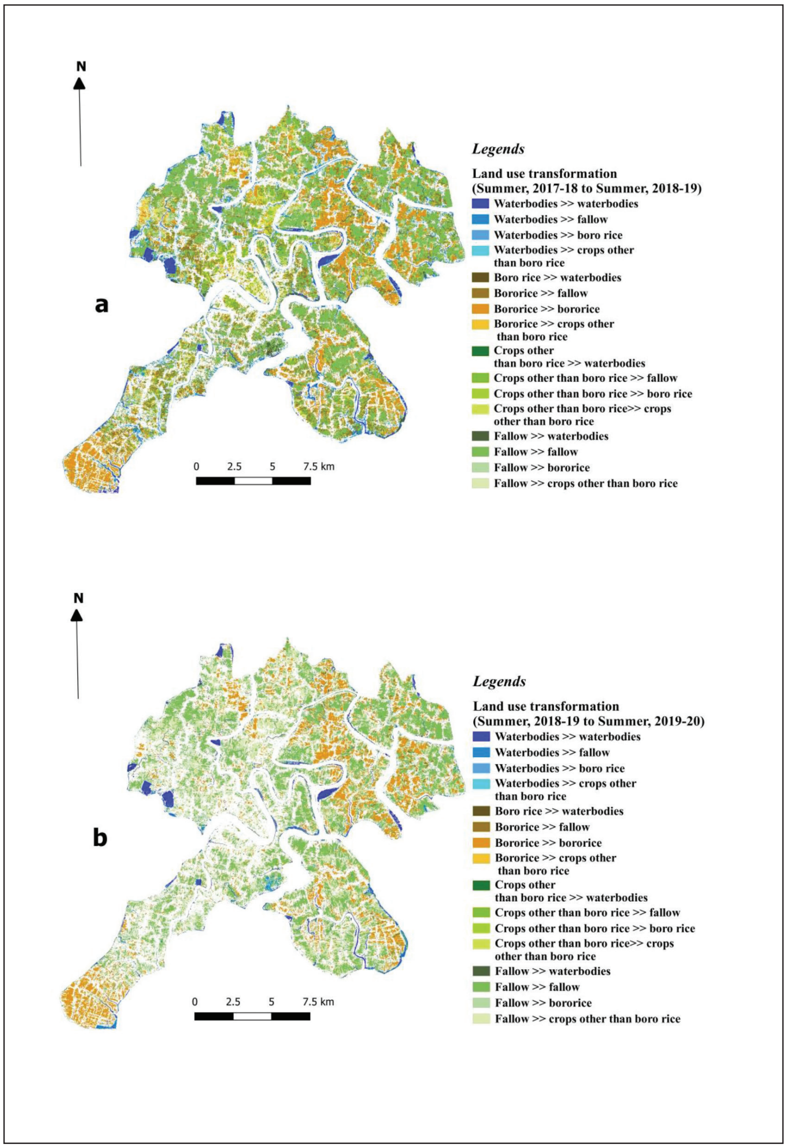

Fig. 8. *Pre-monsoon (summer) season land use transformation a) 2017-2018 to 2018-2019 and b) 2018-2019 to 2019-2020 cropping years*

coverage in 2017-18 was attributed to the good amount of rainfall in October month (375 mm) that made an ample amount of residual soil moisture available for the post-monsoon crops.

Furthermore, the well-distributed light shower in November (24.4 mm), December (51.8 mm), and January (6.2 mm) helped in good growth of the post-monsoon crops. The winter crop coverage was drastically reduced in the following year, 2018-19. The occurrence of tropical cyclone *Bulbul* (Haque *et al.*, 2019) that caused about 600 mm of rainfall in November and waterlogging in the crop fields led to delayed harvesting of *kharif* rice. As a result, post-monsoon crops could not be accommodated. Furthermore, the early sown winter crops, mainly vegetables, were damaged due to waterlogging. The rainfall distribution pattern in the third year of the study (2019-20) showed that the October rain was only 158 mm, followed by negligible rainfall in December and January. This caused a severe shortage of water for growing winter crops.

In the summer season, the farmers cultivated rice, green gram, and some selected vegetables in limited areas. The choice of crops usually depends upon surface water storage (ponds and canals) for irrigation. Besides that, the choice of summer crop is also influenced by the market demand, particularly for green gram. The satellite-based crop coverage mapping revealed a steady increase in area under non-rice crops like green gram and vegetables with a simultaneous decrease in summer rice during 2017-2020. The scattered rain during February and March of 2019 and 2020 helped in successful cultivation of non-rice summer crops like green gram and vegetables. The increase in area under less water demanding non-rice summer crops is a good trend from a sustainability perspective.

The present study demonstrated the usefulness of multi-temporal Sentinel-2 data for estimating crop acreage with higher accuracies. The application of random forest classification as a machine learning technique, with multi-temporal Sentinel-2 imageries as input, proved to be effective in spatio-temporal mapping of seasonal fallow and croplands with high accuracy. Multi-temporal Sentinel-2 data can be used to study crop growth by analyzing the temporal variation in the spectral behaviour of crops. It was evident that the crop, fallow, and tree vegetation could be successfully distinguished by applying multi-temporal Sentinel-2 data. The temporal NDVI profile indicates the initiation and termination of a crop in a particular cropping system. This helps to determine the cropping intensity of any region and to optimize the cropping window towards sustainable cropping system intensification.

The cropping system analysis for three consecutive years (2017-18, 2018-19, and 2019-20) inferred that the rainfall pattern during October to February largely influenced the cropping intensity of the study areas. The conventional practice of long-duration rice cultivation provides limited scope for growing winter crops. The crop production in the coastal blocks of Sundarban is highly vulnerable to hydro-meteorological uncertainties. Good rainfall during the end of the monsoon helped in a successful post-monsoon crop when broadcasted as a relay (*utera*) cropping with rice, whereas cyclonic storms associated with heavy rainfall during November adversely affected the post-monsoon crop. Scattered rain during February-March helped in non-rice summer crops like green gram. The assessment of the cropping scenario through satellite data can help to develop a judicious crop plan to deal with the erratic monsoon, untimely post-monsoon rainfall, and crop damage due to cyclonic storms.

CONFLICTS OF INTEREST

The authors declare no conflicts of interest/competing interests.

ACKNOWLEDGEMENT

We acknowledge the financial support of the Australian Centre for International Agricultural Research (ACIAR) through the project CSI4CZ. The authors are thankful to the Tagore Society for Rural Development (TSRD) for their ground support and the farmers of the Gosaba Block of Indian Sundarbans for their unconditional cooperation.

REFERENCES

Bell, R.W., Mainuddin, M., Barrett-Lennard, E.G., Sarangi, S.K., Maniruzzaman, M., Brahmachari, K. and Hossain, M.B. (2019). Cropping systems intensification in the coastal zone of the Ganges delta: Opportunities and risks. *Journal of the Indian Society of Coastal Agricultural Research* **37**(2): 153-161.

Blesh, J., Hoey, L., Jones, A.D., Friedmann, H. and Perfecto, I. (2019). Development pathways toward “zero hunger”. *World Development* **118**: 1-14. https://doi.org/10.1016/j.world dev.2019.02.004.

Breiman, L. (2001). Random forests. *Machine learning* **45**(1): 5-32.

Debnath, A. (2018). Land use and land cover change detection of Gosaba island of the Indian Sundarban region by using multitemporal satellite image. *International Journal of Humanities & Social Science* **7**(1): 209-217.

Ghosh, A., Nanda, M.K. and Sarkar, D. (2022). Assessing the spatial variation of cropping intensity using multi-temporal Sentinel-2 data by rule-based classification. *Environment, Development and Sustainability* **24**(9): 10829-10851.

Ghosh, A., Nanda, M. K., Sarkar, D., Sarkar, S., Brahmachari, K. and Ray, K. (2019). Application of multi-dated Sentinel-2 imageries to assess the cropping system in Gosaba island of Indian Sundarbans. *Journal of the Indian Society of Coastal Agricultural Research* **37**: 32-44.

Govt. of West Bengal. (2014). *District Statistical Handbook, South 24-Parganas*, Directorate of Bureau of Applied Economics & Statistics, Department of Planning, Statistics & Programme Monitoring, Government of West Bengal, Kolkata, West Bengal, India. http://wbpspm.gov.in/publications/District%20Statistical%20 Handbook.

Haldar, A. and Debnath, A. (2014). Assessment of climate induced soil salinity conditions of Gosaba Island, West Bengal and its influence on local livelihood. In *Climate Change and Biodiversity*, Proceedings of IGU Rohtak Conference, Vol. 1, M. Singh, R.B. Singh and M.I. Hassan (eds.), Springer, Tokyo, Japan. pp 27-44.

Haque, M., Alam, M., Moniruzzaman, S. and Hoque, M. (2019). The impact of climate change in the coastal areas of Bangladesh affected by cyclone Bulbul. *Bangladesh Journal of Extension Education* **31**(1&2): 13-27.

IMD. (2020). *Observed Rainfall Variability and Changes Over West Bengal State*, Met Monograph No.: ESSO/IMD/HS/Rainfall Variability/29(2020)/53, Climate Research and Services, India Meteorological Department, Ministry of Earth Sciences, Govt. of India, Pune, Maharashtra, India.

Mainuddin, M., Bell, R.W., Gaydon, D.S., Kirby, J.M., Barrett-Lennard, E.G., Glover, M., Razzaque Akanda, M.A., Maji, B., Ali, M.A., Brahmachari, K., Maniruzzaman, M., Aziz, M.A., Burman, D., Biswas, J.C., Rahman, M.M. and Sarangi, S.K. (2019a). An overview of the Ganges coastal zone: Climate, hydrology, land use, and vulnerability. *Journal of the Indian Society of Coastal Agricultural Research* **37**(2): 1-11.

Mainuddin, M., Rahman, M.A., Maniruzzaman, M., Sarker, K.K., Mandal, U.K., Nanda, M.K., Gaydon, D.S., Sarangi, S.K., Sarkar, S., Yu, Y., Islam, M.T. and Kirby, M. (2019b). The water and salt balance of polders/islands in the Ganges delta. *Journal of the Indian Society of Coastal Agricultural Research* **37**(2): 45-50.

Mandal, D., Kumar, V., Rao, Y.S., Bhattacharya, A., Bera, S. and Nanda, M.K. (2018). Combined analysis of Radarsat-2 SAR and Sentinel-2 optical data for improved monitoring of tuber initiation stage of potato. *The International Archives of the Photogrammetry*, *Remote Sensing and Spatial Information Sciences* XLII-5: 275-279. https://doi.org/10.5194/isprs-archives-XLII-5-275-2018.

Mondejar, J.P. and Tongco, A.F. (2019). Near infrared band of Landsat 8 as water index: A case study around Cordova and Lapu-Lapu City, Cebu, Philippines. *Sustainable Environmental Research* **29**:16. https://doi.org/10.1186/s42834-019-0016-5.

Ramoelo, A., Cho, M., Mathieu, R. and Skidmore, A.K. (2015). Potential of Sentinel-2 spectral configuration to assess range land quality. *Journal of Applied Remote Sensing* **9**(1): 094096. https://doi.org/10.1117/1.JRS.9.094096.

Ray, K., Brahmachari, M., Goswami, R., Sarkar, S., Brahmachari, K., Ghosh, A. and Nanda, M. K. (2019). Adoption of improved technologies for cropping intensification in the coastal zone of West Bengal, India: A village level study for impact assessment. *Journal of the Indian Society of Coastal Agricultural Research* **37**(2): 144-152.

Rodriguez-Galiano, V.F., Chica-Olmo, M., Abarca-Hernandez, F., Atkinson, P.M. and Jeganathan, C. (2012). Random forest classification of Mediterranean land cover using multi-seasonal imagery and multi-seasonal texture. *Remote Sensing of Environment* **121**: 93-107. https://doi.org/10.1016/j.rse.2011.12.003.

Rouse, Jr.J.W., Haas, R.H., Schell, J.A. and Deering, D.W. (1974). Monitoring vegetation systems in the Great Plains with ERTS. Third Earth Resources Technology Satellite-1 Symposium, Volume I: Technical Presentations, NASA SP-351, S.C. Freden, E.P. Mercanti and M.A. Becker (eds.), NASA, Washington, D.C., USA. pp 309.

Sahu, A.S. (2014). A study on Moyna basin water-logged areas (India) using remote sensing and GIS methods and their contemporary economic significance. *Geography Journal* **2014**: 401234. https://doi.org/10.1155/2014/401324.

Samanta, K. and Hazra, S. (2012). Landuse/landcover change study of Jharkhali Island Sundarbans, West Bengal using remote sensing and GIS. *International Journal of Geomatics and Geosciences* **3**: 299-306.

Sarkar, S., Ghosh, A., Brahmachari, K., Ray, K., Nanda, M.K. and Sarkar, D. (2020) Weather relation of rice-grass pea crop sequence in Indian Sundarbans. *Journal of Agrometeorology* **22**(2): 148-157. https://doi.org/10.54386/jam.v22i2.155.

Sarkar, S., Samui, I., Brahmachari, K., Ray, K., Ghosh, A., and Nanda, M. K. (2019). Management practices for utera pulses in rice-fallow system under coastal saline zone of West Bengal. *Journal of the Indian Society of Coastal Agricultural Research* **37**(2): 98-103.

Stehman, S. (1996). Estimating the kappa coefficient and its variance under stratified random sampling. *Photogrammetric Engineering and Remote Sensing* **62**(4): 401-407.

Veloso, A., Mermoz, S., Bouvet, A., Toan, T.L., Planells, M., Dejoux, J.F. and Ceschia, E. (2017). Understanding the temporal behavior of crops using Sentinel-1 and Sentinel-2-like data for agricultural applications. *Remote Sensing of Environment* **199**: 415-426. https://doi.org/10.1016/j.rse.2017.07.015.